

# Propagation Modes and Temporal Variations along a Lift Shaft in UHF band

Xiao Hong Mao, *Student Member, IEEE*, Yee Hui Lee, *Member, IEEE*,

and Boon Chong Ng, *Senior Member, IEEE*

**Abstract**— The guiding of electromagnetic waves along the lift shaft is studied and presented in this paper. Wideband channel sounding in UHF band along a lift shaft located in a complex environment has been conducted. Based on the measured delay in time of arrival, large structures that cause multipath clusters can be identified. The different propagation mechanisms associated with the lift shaft is then studied in detail. Analysis of the measurement results verifies the presence of electromagnetic waves being guided along the lift shaft. This guiding effect of the lift shaft is significant and is an important propagation mechanism. Temporal variation of the guided waves caused by different components of the lift shaft such as the lift door and the lift car has also been studied. Conclusions drawn from measurement results are validated using 3-D ray tracing simulation results. This research is useful for military applications such as urban warfare.

**Index Terms**—3-D ray tracing, lift shaft, temporal variation, urban area, waveguide effect.

## I. INTRODUCTION

THE field of indoor radio propagation has been well developed since the early 1980s. Studies of indoor radio wave propagation play an important role for system designers. For example, channel characterization in hospital [1] can provide channel information for system planner so as to ensure that hospital staffs are contactable at all times without causing any interference to medical equipments. The lift shaft and its associated lift car create an RF-harsh propagation environment [2]. In fact, the propagation environment of a lift shaft is similar to that of a tunnel or an indoor corridor; topics that are well-studied in the UHF band [3]–[6]. The waveguide mechanism for UHF communication within a tunnel has been identified since 1975 [3]. Subsequently, the mine tunnel has

been modelled as a waveguide for UHF band communication in [4]. In [5], it was concluded from the small path loss obtained that the corridor can exhibit waveguide effects. In [6], the corridor was found to behave like a large waveguide since the measured loss is smaller than the free space path loss. Besides these analogues-waveguide structures, the heating, ventilation and air conditioning (HVAC) ducts in buildings have also been modelled as a multimode waveguide at high frequency [7]. In [7], an approximate propagation model for a straight HVAC duct channel is presented. It is shown that the HVAC duct can be modelled as a multimode waveguide. Due to the similarity in geometry between a lift shaft, a tunnel, an indoor corridor, and a HVAC duct, waveguide effect may also exist in the propagation path along the lift shaft.

Little research work has been done on the effect of propagation within the lift shaft. In [8], the effect of placement and orientation of antenna has been examined for propagation along the lift shaft through FDTD simulations. They concluded that the main mechanism for signal propagation within the lift shaft is independent of polarization. In the following year, the same group of researcher studied the propagation of GSM signals in a lift shaft for network planning purposes [2]. They concluded that, at the higher GSM frequency band of 1800 MHz, although signal propagation is believed to be worse than that at the lower GSM frequency band of 900 MHz, it was found to be approximately 5 dB better. The authors attributed this to the lower energy absorption by the lift car and the people in the lift car in the higher GSM band. They also showed that the vertical lift shaft is an over-sized waveguide and therefore, have a lower attenuation factor in the higher GSM band. However, no further study on the waveguide effect has been conducted. Application focused research works have studied the effect of the moving elevator on the number of handoffs required for effective cell planning purposes [9]. In [2], [8], [9], narrowband measurement has been conducted, with the aim of studying the variation in signal strength of the moving elevator. In [10], impulsive noise measurements for indoor buildings at UHF (918 and 2440 MHz) and microwave (4 GHz) frequencies are conducted and the elevator has been identified as one of the significant sources of impulsive noise. The study shows that as the frequency increases, the impulse noise amplitude and duration decreases.

Manuscript received June 19, 2009; revised January 12, 2010. This work was supported in full by the Advanced Communications Research Program DSOCLO6271, a research grant from the Directorate of Research and Technology (DRTech), Ministry of Defence, Singapore.

X. H. Mao and Y. H. Lee are with the School of Electrical and Electronic Engineering, Nanyang Technological University, Singapore 639798, Singapore (e-mail: xhmao@ntu.edu.sg; eyhlee@ntu.edu.sg).

B. C. Ng is with the Advance Communication Laboratories, Defence Science Organization (DSO) National Laboratories, Singapore and also with the School of Electrical and Electronic Engineering, Nanyang Technological University, Singapore 639798, Singapore (e-mail: ebcng@ntu.edu.sg).

Recently, there has been interest in urban warfare. It is critical for soldiers to be able to communicate with each other reliably during war time [11]. However, there is little published literature on communication in urban areas in the military UHF band of 225 to 400 MHz. In this paper, wideband channel sounding is performed at 255.6 MHz in order to understand the propagation mechanisms over a lift shaft within an urban environment. Channel measurement is performed in the frequency domain. The time domain channel response is derived from the frequency response of the channel for analysis. This wideband sounding aims to identify the propagation mechanisms for communication along a lift shaft within a complex environment. More importantly, the waveguide effect associated with the lift shaft will be examined. The temporal variation on the guided waves caused by the lift door and the lift car is studied in detail. To validate the measurement results, 3-D ray-tracing simulation is performed and results are compared.

This paper consists of three sections. Section II describes the measurement environment, measurement setup, as well as the simulation scenarios. In Section III, results obtained from measurement and simulation are presented, compared and analysed. Based on the analysis, propagation modes and temporal variations are discussed. This is followed by the conclusions of the findings in Section IV.

## II. CHANNEL MEASUREMENT AND SIMULATION

### A. Measurement Sites

Measurements have been conducted along a lift shaft in an education building in Nanyang Technological University, Singapore in June, 2008. This education building is 7-storey high and is known as block S2. Each level (except level 7) in block S2 is about 3.9 m in height and it consists of three main blocks. Inside each block are laboratories, except for level 6 where there are offices. There are open walk ways that runs along all the 3 blocks on both sides of the building as seen in Fig. 1(a). These open walk ways have concrete railings. The walls of the 3 main blocks are made of concrete and on the side walls facing the two walk ways are glass windows. All doors in the building are made of heavy wood. The ceilings along the walk ways are lined with thin aluminium plates. The lift shaft under study has concrete walls that spans 7 levels and is situated between the middle block and the last block in the building S2. On the opposite side



Fig. 1. Experimental environment. (a) Location of antenna. (b) Surrounding environment of the experimental site.

of the lift shaft, there is a stairwell of the same height. Throughout the experiment, the location of the transmitter and the receiver are fixed at level 3 and level 6, respectively. The antennas are placed directly outside of the lift door as shown in Fig. 1(a). From Fig. 1(b) it can be seen that there is a building in the surrounding environment known as block S1 which is identical and in parallel to block S2 (the experimental site) at a distance of 78 m away. There is also another group of education buildings known as the Communication School (CS) which is situated between block S1 and block S2 as seen in Fig. 1(b). The material of the blocks CS and S1 are similar to that of block S2. In order to identify the reflections from surrounding buildings on the propagation paths, controlled experiments are conducted. A metallic plate of dimensions, 2.3 m by 1.3 m by 3 mm (Length x Width x Depth) is placed along the corridor to prevent the signal from propagating out of block S2 towards the surrounding buildings. After identifying the reflections from surrounding buildings, the propagation mechanisms associated with nearby environment such as the lift shaft can be isolated for analysis. The propagation mechanism within the lift shaft is then examined through a series of experiments with the lift door opened or closed and with the lift car situated at different levels within the lift shaft. The temporal variations of the guided wave can then be studied.

### B. System Setup

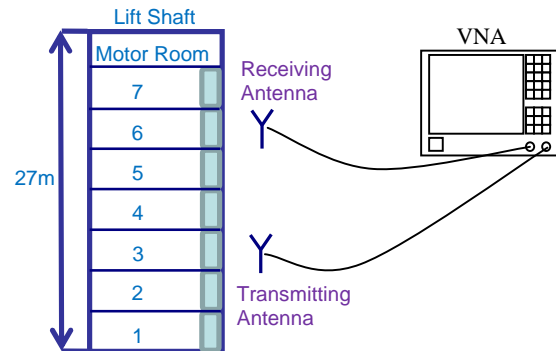


Fig. 2. Schematic diagram of the measurement setup.

Three wideband channel sounding techniques namely; direct pulse measurements; spread spectrum sliding correlator measurements; and swept frequency measurements are reported in [12]. Of the three sounding techniques, the swept frequency measurement is used because of its ability to achieve a high resolution. The measurement system consists of an Agilent Vector Network Analyser (VNA) and two identical Discone antennas AX-71C (Fig. 1(a)). Fig. 2 shows the schematic diagram of the experiment setup. The centre frequency is fixed at 255.6 MHz and 1601 uniformly distributed continuous waves are transmitted over a bandwidth of 300 MHz. With this specification, the highest resolvable path difference is 1 m and the maximum excess delay is 5.33  $\mu$ s. To ensure that the channel is static during a single sweep of the measurement, the minimum sweep time of 111.56 ms is used. It is noted that the minimum sweep time is proportional to the number of points (1601) and inversely proportional to the intermediate frequency bandwidth of 3 kHz for the Agilent

E5062A VNA. For each measurement, a set of 50 sweeps are taken and logged via the general purpose interface bus (GPIB) onto a laptop. In order to obtain the time domain channel response, post-processing is done by taking the inverse fast fourier transform (IFFT) of the recorded frequency domain transfer function as shown in (1) and (2).

$$S_{21}(\omega) \propto H(\omega) = \frac{Rx(\omega)}{Tx(\omega)} \quad (1)$$

$$h(t) = FT^{-1}[H(\omega)] \quad (2)$$

### C. Simulation Setup

In this paper, a trial version of the ray-tracing simulator “Wireless Insite [13]” is used to obtain detailed channel information. The ray-tracing scenario presented is a simplified model of the actual environment and the 3-D model is simulated to address the effect of transmission, reflection, and diffraction. The applied simulation model is developed based on a hybrid shooting bouncing ray (SBR) algorithm and geometrical theory of diffraction (GTD). The SBR method is implemented with robust ray tracing techniques where once the propagation paths are found, the field is evaluated by far-field transmission and reflection coefficients. The amplitudes of the diffracted fields are evaluated by GTD [13]. In the basic form of the SBR technique, it is assumed that the incident electromagnetic wave is planar and is partitioned perpendicularly into a large number of ray tubes such that any particular ray tube will initially intersect with a small area of the whole target. The ray tubes are required to be spaced sufficiently finely so that other simplifying assumptions i.e. ray remaining planar and the shape remaining circular can remain valid throughout the full ray path. For this simulator, the ray spacing can be specified by the user based on the application. However, fine ray spacing can lead to long computation time. The advantage of the SBR algorithm is its simplicity, but the model is less effective when the target features are complex and there are multiple scatters in more than one direction [14][15].

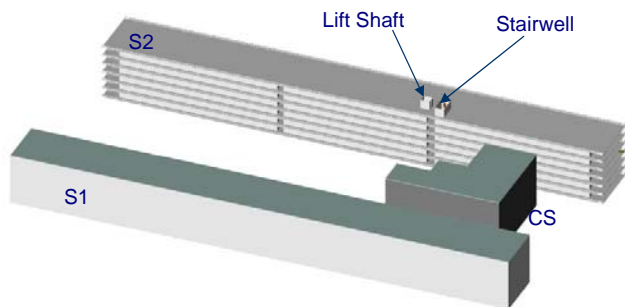


Fig. 3. 3D simulation scenario.

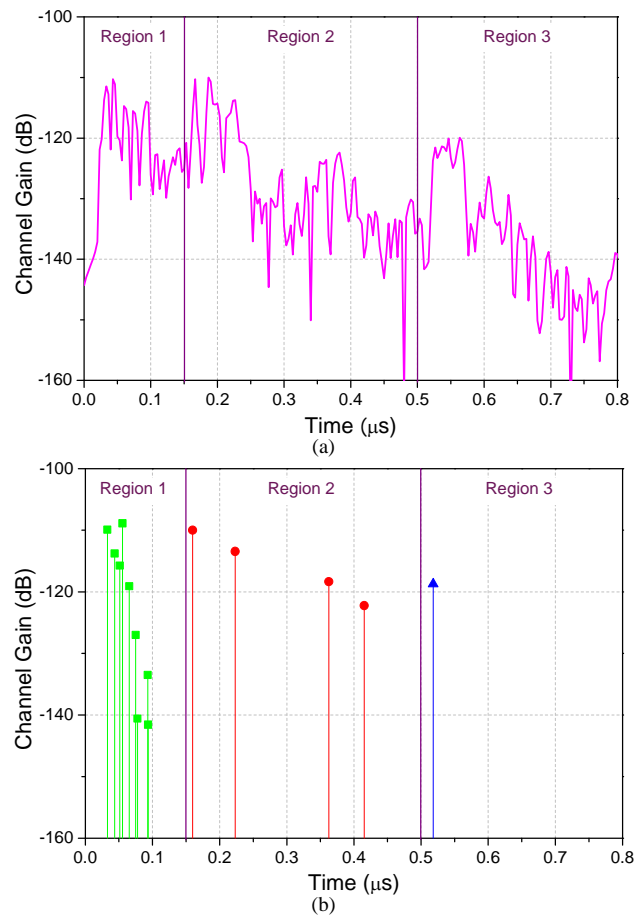
Fig. 3 shows the simulation scenario with the lift shaft under investigation in block S2, and the surrounding blocks S1 and CS. The material of the walls of all the buildings is modeled using layered drywall, while the floors and ceilings are modeled using concrete. For each level, two railings with a

height of 1 m are added. The lift shaft and the stairwell are modeled as a series of empty rooms which spans 7 levels, and the lift car is modeled as a hollow metallic box. Vertically polarized omni-directional dipoles are used as the transmitting and receiving antennas. The simulated power differences between the different rays/multipaths are compared to the measured ones. For ease of comparison, all powers in the simulations are normalized to the measured power. The maximum reflection is set to 2 and the maximum transmission is set to 10. For each simulation, Wireless Insite is able to generate a list of propagation paths (up to 250 rays) and the amplitudes associated with the paths.

## III. RESULTS AND DISCUSSION

### A. Overview of the Power Delay Profile

Fig. 4(a) shows the measured time domain channel response when the transmitter is at level 3 and the receiver is at level 6 while the lift car is kept stationary at level 3. The power delay profile can be classified into three regions indicated by the vertical lines. Region 1 range from 0 to 0.15  $\mu\text{s}$  on the time axis, region 2 range from 0.15 to 0.5  $\mu\text{s}$  while region 3 is for a time of 0.5  $\mu\text{s}$  and above. Fig. 4(b) shows the simulated power delay profile with the different rays identified by the simulator. Similarly, the simulated rays are classified into 3 regions according to their time of arrival. Comparing the two figures,



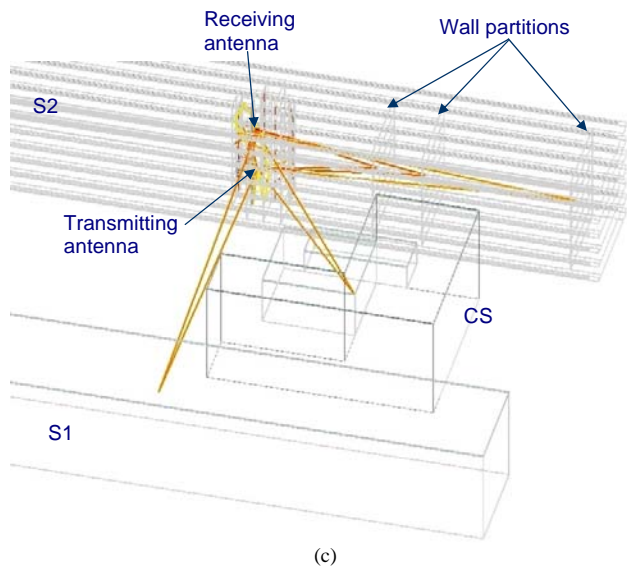


Fig. 4. (a) Measured power delay profile. (b) Simulated ray tracing power delay profile. (c) 3D visualization from simulator.

the propagation mechanism associated with each region can be analyzed with the help of the ray visualization shown in Fig. 4(c). It is identified that rays in region 3 and region 2 are a result of signals being reflected off obstacles in the far region (block S1) and the intermediate region (block CS and far ends of block S2). The loss-distance relationship in region 1 indicates the possible sources of signals; they are the direct signal that penetrates through the ceilings and floors; the signal that are reflected and/or diffracted by nearby objects; and more importantly, the signal that enters the lift shaft, and propagates within the lift shaft to the receiver. The propagation within each region is further analyzed in the sections *B* to *E*. In section *B*, the far and intermediate reflectors are identified through measurements and simulations. In section *C*, the nearby environment especially the temporal variations associated with the lift shaft is examined in detail. In section *D*, a comparison of the average channel gain for different measurement scenarios are presented. Finally in section *E*, the root-mean-square (rms) delay spread for all measurement scenarios are discussed.

### B. Propagation Mechanism of Signals in Region 3 and 2

By examining the time of arrival of the signals within region 3 and region 2, it can be concluded that signals in these two regions are a result of reflections by large static obstacles in the far and intermediate regions. In this measurement campaign, there are two clusters of buildings (block S1 and block CS) situated on the left-hand side of the block S2. In order to identify the reflections from these buildings, a set of controlled experiments are conducted by placing a metallic plate on the left-hand side of the corridor at the level of the transmitter. This metallic plate serves to reduce the number of signals propagating out of the corridor towards the far and intermediate reflectors.

Fig. 5(a) shows a comparison of measured channel response with and without the metallic plate. It is observed that when the metallic plate is present, the strength of signals received within

region 2 (except the first two clusters of peaks) and region 3 decrease by up to 7.7 dB. This verifies that region 3 and region 2 contain signals reflected from the far region of block S1 and the intermediate region of block CS. The unchanged amplitude of the first two clusters of peaks in region 2 is due to the reflections of intermediate reflectors within block S2 and the incomplete blocking due to the limited size of the metallic plate.

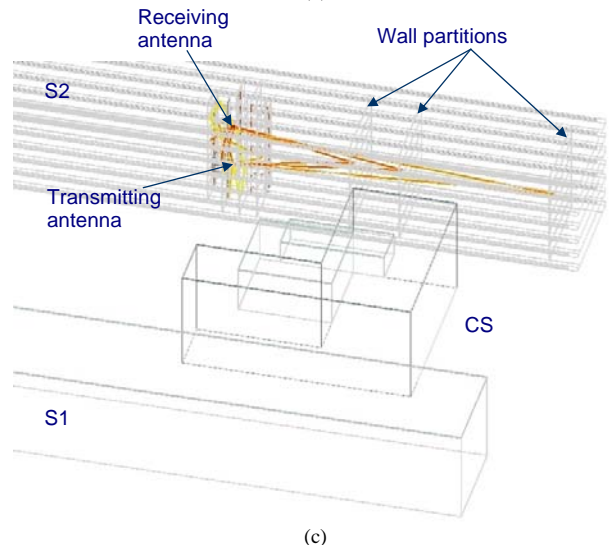
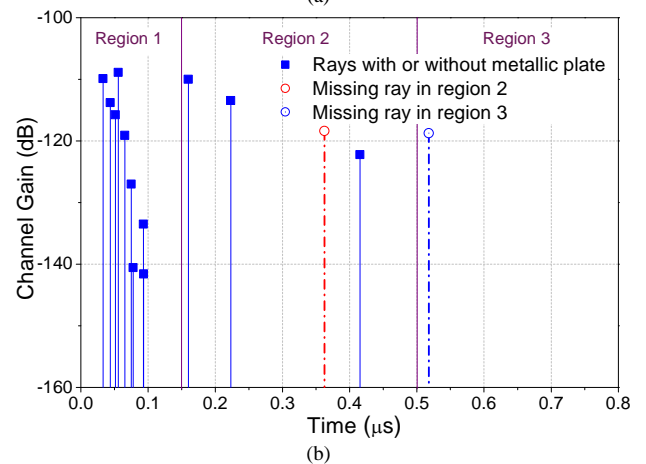
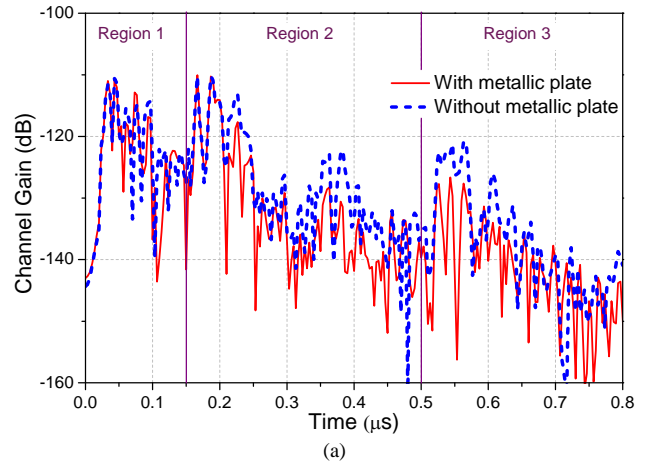


Fig. 5. Metallic plate at transmitter level. (a) Measured power delay profile. (b) Simulated ray tracing power delay profile. (c) 3D visualization from simulator.

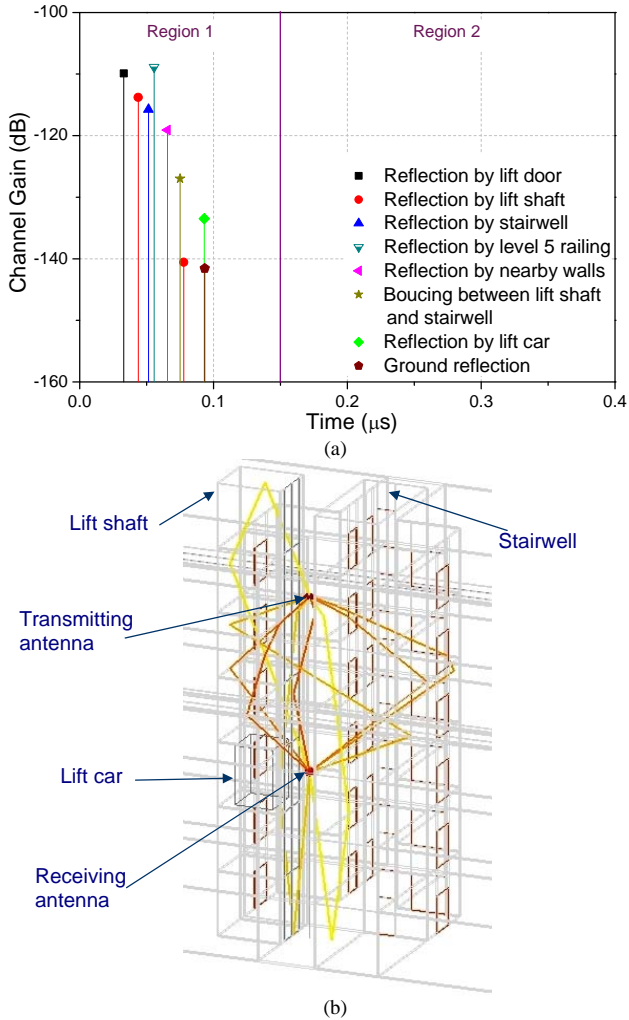


Fig. 6. Nearby environment. (a) Simulated ray tracing power delay profile. (b) 3D visualization from simulation.

A perfect electric conductor board is used to block the same side of the corridor in the simulation. Fig. 5(b) shows the simulated power delay profile. The dotted impulses indicate the rays that are absent when the metallic plate is placed in the corridor. The red dotted impulse represents the signal reflected from the block CS whereas the blue dotted impulse represents the signal reflected off the block S1. Comparing Fig. 5(c) and Fig. 4(c), it is observed that rays reflected from the block CS and the block S1 are missing when the metallic plate is placed in the corridor in the simulation. As shown in Fig. 5(b), there are three remaining multipath rays in region 2 when the metallic plate is placed in the corridor. These three rays are a result of reflections from the wall partitions within block S2.

From these measurement and simulation results, the far and the intermediate reflectors are identified. Next, the nearby propagation mechanisms are analysed.

### C. Propagation Mechanism of Signals in Region 1

Fig. 6(a) shows the rays within region 1 from the simulator. These rays can be further classified into eight different propagation mechanisms. As expected, region 1 includes signal penetrating through the floors and ceilings, signal reflected

and/or diffracted by nearby objects such as the lift door, walls and railings, and most importantly, signal guided by lift shaft. A similar wave guiding effect is observed for the stairwell. Fig. 6(b) provides the visualization of the above mentioned propagation paths. In order to study the waveguide effect of the lift shaft, controlled experiments are conducted by keeping the lift door opened and closed at the transmitter level and the receiver level; and by varying the position of the lift car from level 1 to level 7 (with the lift door closed). For all of the three sets of experiments, the transmitter and the receiver are fixed at level 3 and level 6, respectively. These experimental results are verified through the simulation of an isolated lift shaft with a lift car within the lift shaft as shown in Fig. 7. In order to aid analysis, only simulated rays that are not common between the two simulations are shown in the PDPs and the visualizations.

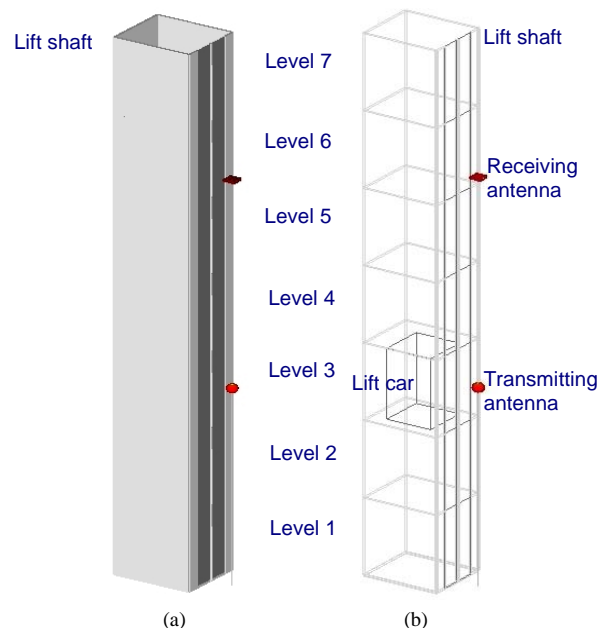


Fig. 7. Simulation scenario of the lift shaft in (a) solid view and (b) transparent view.

1) *Lift Door Effect*: Fig. 8(a) shows the measurement result obtained when the lift door is opened and when the lift door is closed at the transmitter level. It is observed that almost all the resolvable signals within region 1 are affected by the opening and closing of the lift door and the strength of these signals are approximately 14 dB higher when the lift door is opened. This indicates that region 1 contains signals that enter the lift shaft from the lift door and then propagate along the lift to the receiver. Based on the diffraction theory, when the lift door is open, the door opening is larger than the wavelength, and therefore, the waves can propagate directly into the lift shaft. When the lift door is closed, the width of the slit in the door is small compared to the wavelength, and therefore, waves are diffracted into the lift shaft via the rubber seal. This results in a diffraction loss that can be as much as 14 dB. Fig. 8(b) shows the simulation results for the lift shaft when the lift door is opened and when the lift door is closed (common rays not shown). Figs. 8(c), and (d) show the corresponding visualization of rays that result in the impulse responses in Fig.

8(b). By comparing the impulse responses in Fig. 8(b) with the lift door opened and with the lift door closed, it is observed that,

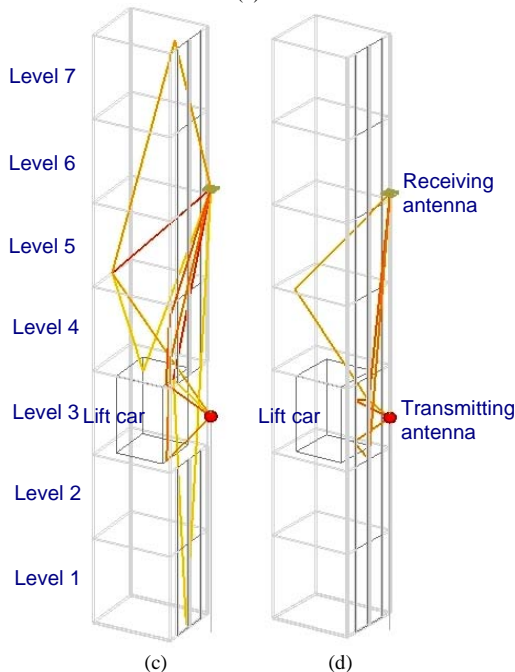
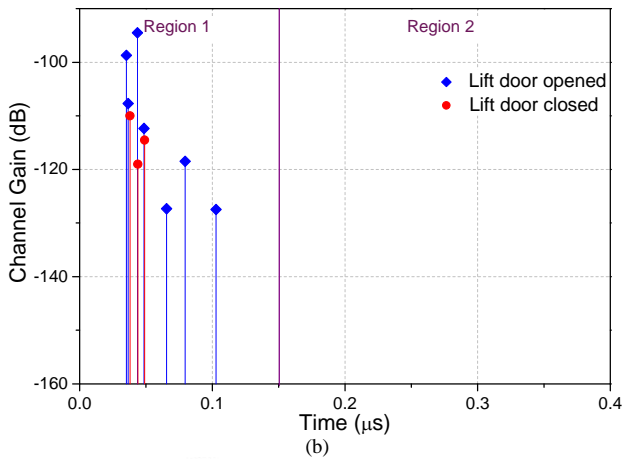
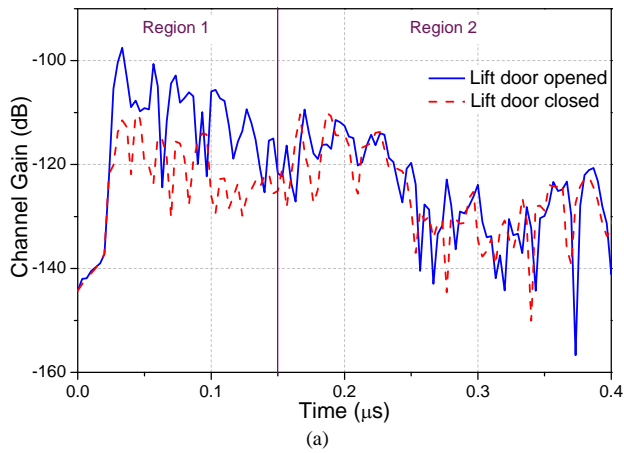
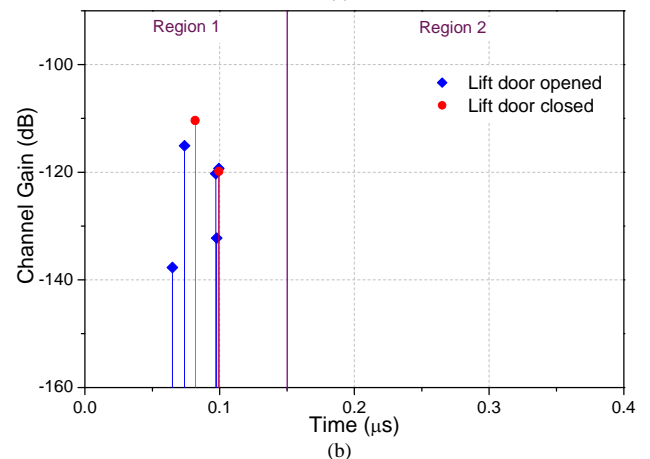
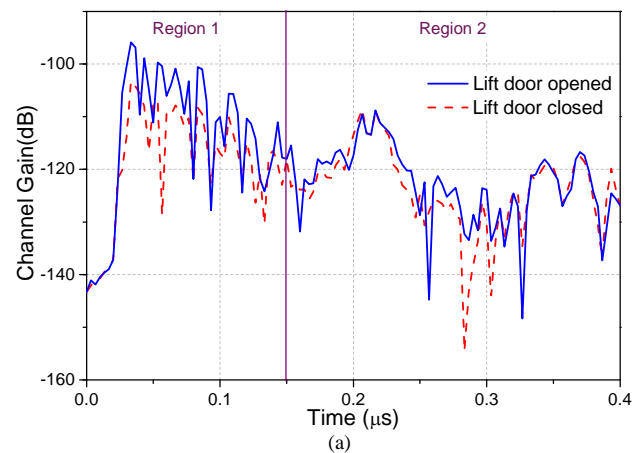


Fig. 8. Open-close lift door at transmitter level. (a) Measured power delay profile. (b) Simulated ray tracing power delay profiles. (c) 3D visualization from simulator for lift door open. (d) 3D visualization from simulator for lift door closed.

the lift door stops a significant number of rays from entering the lift shaft. This accounts for the diffraction loss observed in the measured results shown in Fig. 8(a). By examining the number of rays in Figs. 8(c), and (d), it can be seen that, there is a reduction in the number of rays reflected and guided by the lift shaft when the door is closed. With the lift door closed, due to the perfect electric conducting lift door in the simulator, no signal can penetrate through the lift door. The gap of the lift door is modeled using a slit (free space) in the middle of the perfect conducting lift door; signals can leak through or be diffracted by the slit and enter the lift shaft. Therefore, the amount of rays guided by the lift shaft is reduced significantly as shown in Fig. 8(d).

A similar analysis has been performed in order to examine the effect of the lift door (opened and closed) at the receiver level (level 6). Fig. 9(a) shows the power delay profile obtained through experiments by opening and closing lift door at the receiver level. Fig. 9(b) shows propagating rays (common rays not shown) from the simulation results, while Figs. 9(c) and (d) provides visualization for rays in Fig. 9(b). As expected, more signals can propagate out from the lift shaft with higher signal strengths due to the open door at the receiver level. From the measured results, the maximum difference is approximately 7.6 dB. This is significantly less than that obtained by opening and closing the lift door at the transmitter level (14 dB). A similar conclusion can be drawn from the simulation results. When the



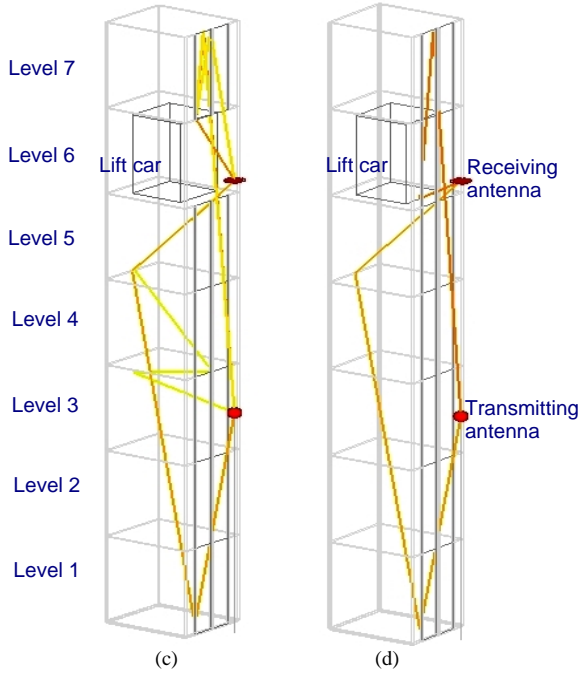


Fig. 9. Open-close lift door at receiver level. (a) Measured power delay profile. (b) Simulated ray tracing power delay profiles. (c) 3D visualization from simulator for lift door open. (d) 3D visualization from simulator for lift door closed.

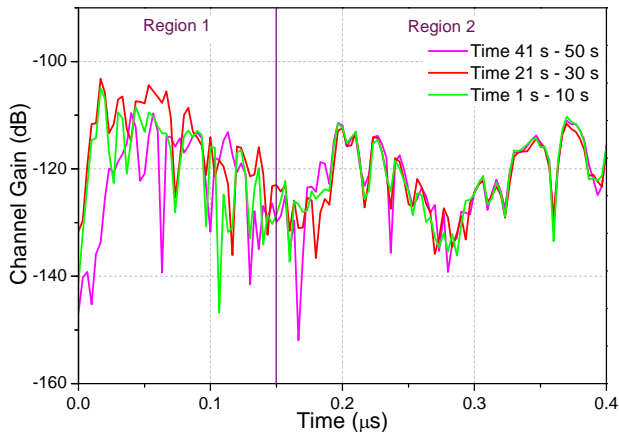


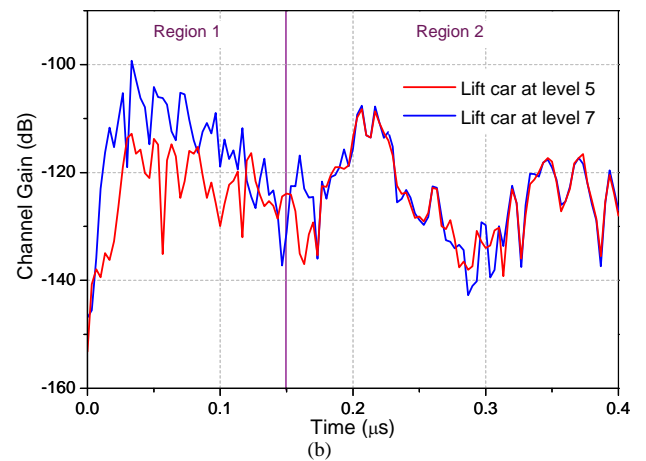
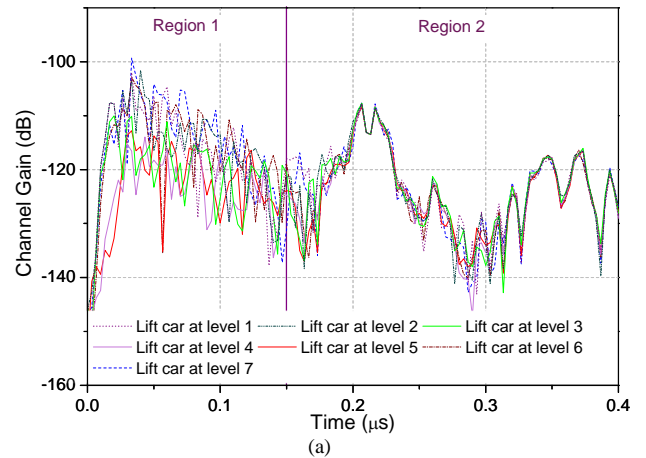
Fig. 10. Measured power delay profile when the lift car is moving.

lift door is opened at the transmitter level, fewer rays are affected, meaning there is less ray difference in Figs. 9(c) and (d) whereas when lift door is opened at the transmitter level, more rays are affected, meaning there is more ray difference in Figs. 8(c) and (d).

As shown in both simulation and the measurement results, the status of the lift door can cause temporal variations to the guided signals. A closed lift door at the transmitter level can result in a signal strength variation as much as 14 dB, whereas that at the receiver level results in a much lower signal strength variation of 7.6 dB.

2) *Attenuation Induced by Lift Car*: Fig. 10 shows the temporal variation of the signals guided by the lift shaft when the lift car is moving. These plots are obtained by averaging data files over different period of times. The data files are recorded when the lift is in use and moving along the lift shaft.

As can be seen in Fig. 10, the temporal variations caused by small movement of the lift car within the propagation path can lead to significant small-scale fading. Therefore, a series of controlled experiments are conducted to examine the effect of the lift car on the lift-shaft guided waves. Fig. 11(a) shows the measurement results when the transmitter is at level 3 and the receiver is at level 6, and the position of the lift car is varied from level 1 to level 7, one level at a time and the lift door is closed at all times. It can be seen that the channel gain for the signals in region 1 is the lowest when the lift car is at level 4 and level 5, while the channel gain is the highest when the lift car is at level 1, level 2 and level 7. This is because, when the lift car is at level 1, level 2 or level 7, it is not within the propagation path, therefore, leaving the wave guiding channel empty. Thus, there is no attenuation due to the obstruction of the guided waves by the lift car within the channel. This leads to the high channel gain. When the lift car is at level 4 and level 5, it is in the middle of the propagation path, and therefore, induces significant attenuation to the guided signal. Fig. 11(b) shows the power delay profile of the two extreme cases when the lift result of the effect of the lift car position is shown in Fig. 11(c) (common rays not shown) visualization of the rays is shown in Figs. 12(a), and (b). From Fig. 11(c), it is clear that the empty path between the transmitter and the receiver allows a significant amount of rays to be reflected and guided by the lift shaft to the receiver. When the lift car is in the middle of the



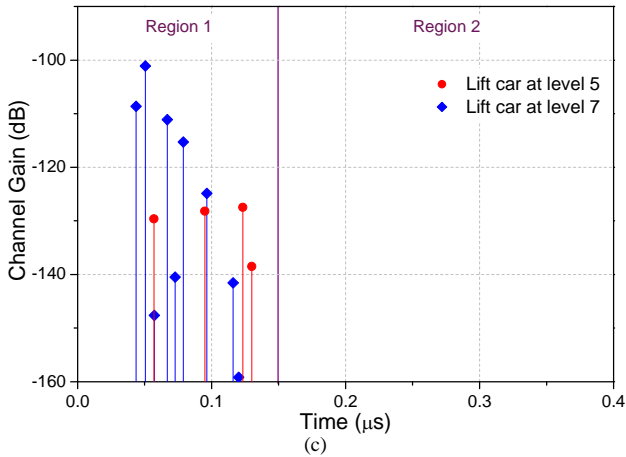


Fig. 11. Variation of lift car position. (a) Measured power delay profile. (b) Power delay profiles when lift car is at level 5 and at level 7. (c) Simulated ray tracing power delay profile.

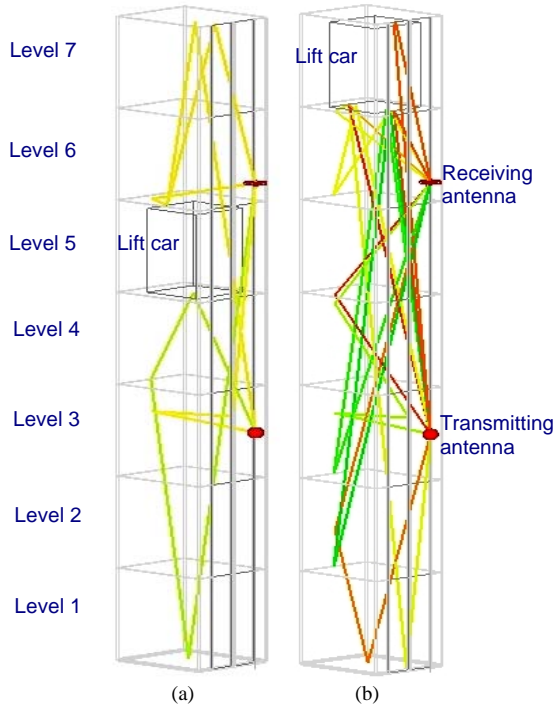


Fig. 12. Variation of lift car position. (a) 3D visualization from simulator for lift car at level 5. (b) 3D visualization from simulator for lift car at level 7.

propagation path, the path is obstructed and signals are attenuated by the lift car. Therefore, there is a significant difference in the number of rays guided along the lift shaft as shown in Figs. 12(a), and (b). Measurement and simulation results in Fig. 11 & Fig. 12 demonstrate both the guiding effect of the lift shaft and the temporal variation to the guided waves due to the movement of the lift car.

#### D. Channel Gain

From the previous sections A, B, and C, it can be concluded that region 1 mainly consists of signals entering the lift door and then guided through the lift shaft to the receiver. The status of the lift door and the position of the lift car will affect the propagation of the signals within region 1. Besides being

guided along the lift shaft in the near region (region 1), signals can be reflected by objects in the intermediate and further regions, shown in region 2 and 3 respectively. In this section, the average channel gain in the three different regions are compared and analyzed. Different measurement scenarios are considered in order to study the effect of the lift door and the effect of the position of the lift car. Table I summarizes the average channel gain within different regions when the lift door is opened/closed at the transmitter and the receiver level (corresponding PDPs shown in Fig. 8(a) & Fig. 9(a)). It is observed that the average channel gain in regions 2 and 3 are not affected by the status of the lift door, whereas the channel gain in region 1 depends a lot on the status of lift door as discussed in section C1. By comparing the channel gains in the three regions in Table I, it can be concluded that, signals in region 1 has the highest channel gain (at least 4.8 dB above that of region 2) and the signals in region 3 have the lowest channel gain due to the longest propagation distance.

TABLE I  
CHANNEL GAIN FOR OPENING/CLOSING LIFT DOOR

Channel gain (dB)	Door closed	Door opened	Door closed	Door opened
	at transmitter level (level 3)		at receiver level (level 6)	
	Region 1	-113.3	-103.4	-109.3
Region 2	-118.1	-118.0	-117.6	-117.5
Region 3	-122.8	-122.6	-123.3	-123.0

The variation of channel gain in the three regions as the position of the lift car is varied, is shown in Fig. 13 (corresponding PDP shown in Fig. 11(a)). It is observed that the channel gain of region 1 is the highest amongst the 3 regions regardless of the position of the lift car. The standard deviations of the average gain for the 3 regions are 4.3, 0.6, and 0.3, respectively. This shows that the channel gain of region 2 and 3 are independent of the position of the lift car, whereas the channel gain of region 1 varies a lot depending on the position of lift car as discussed in section C2. From this analysis it can be concluded that since the channel gain in region 1 is always high, the wave-guiding effect of the lift shaft is an important propagation mechanism in this complex environment. And it is

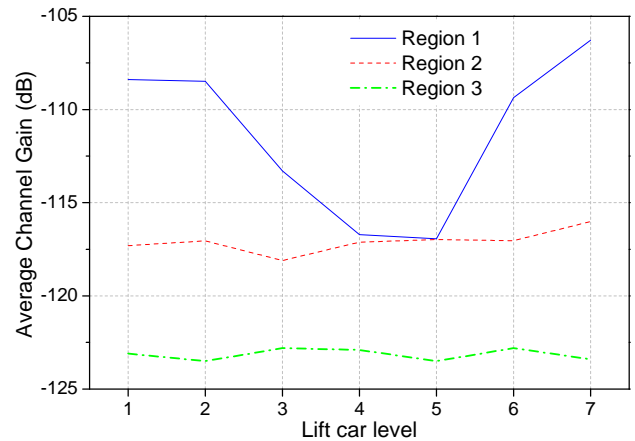


Fig. 13. Average channel gain for different lift car level.

important to understand the temporal variations induced by the lift door and the lift car.

E. RMS Delay Spread

TABLE II  
RMS DELAY SPREAD FOR OPENING/CLOSING LIFT DOOR

RMS delay spread (ns)	Door closed	Door opened	Door closed	Door opened
	at transmitter level (level 3)		at receiver level (level 6)	
	159.2	80.5	127.3	73.4

The rms delay spread values ( $\tau_{rms}$ ) for the scenario when the lift door is opened/closed at the transmitter level and the receiver level are tabulated in Table II. The mean PDPs used for delay spread calculation are obtained by taking an average in the time domain of 50 continuous sweeps at a single position. All signals in the mean PDP with amplitude of at least 5 dB above the noise floor (a threshold of 5 dB signal-to-noise ratio) are considered to be significant peaks. These significant peaks will then be accounted for towards the calculation of the rms delay spread. In Table II, it can be seen that the status of the lift door has significant effect on the rms delay spread as it is determined by the signals' amplitudes and their corresponding time delays. When the lift door is closed, the signal strength and number of rays guided along the lift shaft decreases, while the signals in regions 2 and 3 arriving with a longer delay remain unchanged, therefore, resulting in a longer delay spread. The rms delay spread for different position of the lift car is plotted in Fig. 14 (blue solid line). The delay spread varies with the position of the lift car. When the lift car is in the middle of the propagation path (level 3, 4 and 5), the guided signals are attenuated by the lift car. Therefore, a high rms delay spread of 159 ns is obtained. When the lift car is out of the wave guide (lift shaft), the rms delay spread is smaller.

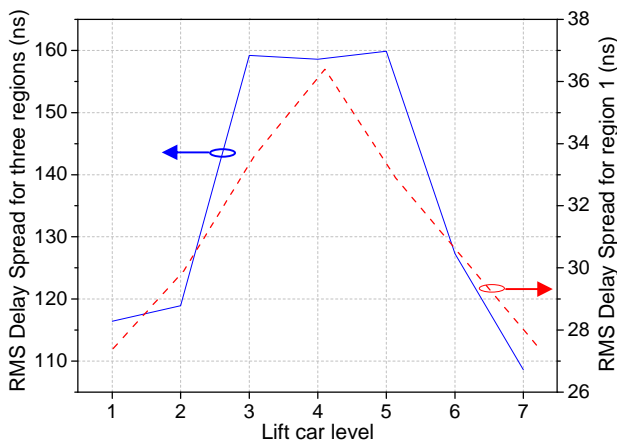


Fig. 14. RMS delay spread for different lift car level.

Taking all the measurement results into consideration, the mean rms delay spread is 122.3 ns. This delay spread is similar to those found in suburban environment [16] but larger than those reported in the literature for propagation along analogues-waveguide structures [17],[18]. In [16], approximately 80% of the rms delay spread values obtained

from channel characterization in the 788-794 MHz band in suburban areas is below 200 ns. In [17], it is reported that the rms delay spread is less than 32 ns for about 50% of the measurement results in an underground mine at 2.4 GHz. In [18], delay spread for propagation in a mine environment in the frequency band of 400 to 500 MHz is within the range of 5-42 ns. The large delay spread reported in this paper is because this calculation has taken into consideration multi-paths in all 3 regions (the wave guided along the lift shaft in region 1 and the open space propagation in regions 2 and 3). If only the delay spread of region 1 is considered, the delay spread for different lift car level is presented in Fig. 14 by the red dotted line. As can be seen, the average value is approximately 31 ns, which is similar to those reported in the literature for analogous waveguide structures [17],[18].

IV. CONCLUSION

In this paper, channel responses from wideband measurements along a lift shaft in a complex university environment have been presented. The corresponding ray-tracing simulations have been performed to verify the measurement results and to identify and visualize the propagation mechanisms. From the channel response obtained, signals have been classified into three regions, and propagation mechanism associated with each region has been discussed. The far and intermediate reflectors have been identified and verified via a set of controlled experiments and their corresponding simulations. Detailed examination of propagation mechanism in nearby region is conducted. It is found that the wave guided along the lift shaft is the main mode of propagation in the urban environment. Through a series of controlled experiments and corresponding simulations, the effect of the lift door and the effect of the position of the lift car are examined. By examining the channel gain and the delay spread, it can be concluded that the lift shaft provides the main propagation mechanism in the complex urban environment. The lift door and lift car induces temporal variation to the guided signals. The opening and closing of the lift door can result in as much as 14 dB of signal variation, while the movement of the lift car can result in a temporal variation of signal strength of up to 13.5 dB. The change in position of the receiving antenna by up to one wavelength has no significant effect on the average channel gain and the rms delay spread, although the signal level for individual resolvable components varies due to the small-scale effects. However, characterization of the small-scale effect is beyond the scope of this paper.

In summary, the lift shaft functions as a waveguide, and is the primary propagation channel in a complex environment. In an environment where propagation is difficult, the waveguide effect of the lift shaft can be an important communication channel. This study of military UHF signal propagation in an urban complex environment is important for military application such as urban warfare. These results and analysis can also be applied to higher frequency applications such as GSM and wireless LAN. For waveguide propagation at high frequencies, the multi-modal interaction can result in rapid

fluctuation in the electric fields. However, for far region waveguide propagation at high frequencies, the dominant-propagation mode suffers a lower falling rate (attenuation per unit length) [19] and therefore, less attenuation.

#### ACKNOWLEDGMENT

The authors are grateful to Anonymous Reviewers and the Associate Editor for their constructive comments and suggestions for the paper.

#### REFERENCES

- [1] T. M. Schafer, J. Manurer, J. V. Hagen and W. Wiesbeck, "Experimental characterization of radio wave propagation in hospitals," *IEEE Trans. Electromagnetic Compatibility*, vol. 47, pp. 304-311, May 2005.
- [2] H. Meskanen and J. Huttunen, "Comparison of a logarithmic and a linear indoor lift car propagation model," in *IEEE Int. Conf. on Personal Wireless Communication*, Jaipur, India, Feb. 1999, pp. 115-120.
- [3] A. G. Emslie, R. L. Lagace, and P. F. Strong, "Theory of the propagation of UHF radio wave in coal mines," *IEEE Trans. Antennas Propagat.*, vol. AP-23, pp. 192-205, May 1973.
- [4] B. L. F. Daku, W. Hawkins, and A. F. Prugger, "Channel measurements in mine tunnels," in *Vehicular Technology Conference*, Birmingham, U.S.A., May. 2002, pp. 380-383.
- [5] K. Giannopoulou, A. Katsareli, D. Dres, D. Vouyioukas and P. Constantinou, "Measurements for 2.4 GHz spread spectrum system in modern office buildings," in *Electrotechnical Conference*, Lemesos, Cyprus, May 2000, pp. 326-329.
- [6] U. Dersch, J. Troger, and E. Zollinger, "Multiple reflections of radio waves in a corridor," *IEEE Trans. Antennas Propagat.*, vol. 42, pp. 1571-1574, Nov. 1994.
- [7] P. V. Nikitin, D. D. Stancil, A. G. Cepni, O. K. Tonguz, A. E. Khafa and D. Brodtkorb, "Propagation model for the HVAC duct as a communication channel," *IEEE Trans. Antennas Propagat.*, vol. 51, pp. 945-951, May 2003.
- [8] H. Meskanen and O. Pekonen, "FDTD analysis of field distribution in an elevator car by using various antenna positions and orientations," *Electronics Letters*, vol. 34, pp. 534-535, Mar. 1998.
- [9] T. S. Kim, H. S. Cho and D. K. Sung, "Moving elevator-cell system in indoor buildings," *IEEE Trans. Vehicular Technology*, vol. 49, pp. 1743-1751, Sep. 2000.
- [10] K. L. Blackard, T. S. Rappaport, and C. W. Bostian, "Measurements and models of radio frequency impulsive noise for indoor wireless communications," *IEEE Journal on Selected Areas in Communication*, vol. 11, pp. 991-1001, Sep. 1993.
- [11] J. R. Hampton, N. M. Merheb, W. L. Lain, D. E. Paunil, R. M. Shuford and W. T. Kasch, "Urban propagation measurements for ground based communication in military UHF Band," *IEEE Trans. Antennas Propagat.*, vol. 54, pp. 644-654, Feb. 2006.
- [12] T. S. Rappaport, *Wireless Communication: Principles and Practice*. New Jersey: Prentice Hall, 2002, ch. 5.
- [13] [Online]. Available: <http://www.remcom.com/wirelessinsite>
- [14] P. E. R. Galloway and T. D. Welsh, "Extensions to the shooting bouncing ray algorithm for scattering from diffusive and grating structures," in *Proc. International Radar Symposium, IRS*, Berlin, Sep. 2005.
- [15] H. Ling, S. W. Lee and R. C. Chou, "High frequency RCS of open cavities with rectangular and circular cross sections," *IEEE Trans. Antennas Propagat.*, vol. 37, pp. 648-654, May 1989.
- [16] A. Semmar, J. Y. Chouinard, V. H. Pham, X. B. Wang, Y. Y. Wu and S. Lafleche, "Digital Broadcasting television channel measurements and characterization for SIMO mobile reception," *IEEE Trans. Broadcasting*, vol. 52, pp. 450-463, Dec. 2006.
- [17] C. Nerguizian, C. L. Despains, S. Affes and M. Djadel, "Radio-channel characterization of an underground mine at 2.4 ghz," *IEEE Trans. Wireless Communication*, vol. 4, pp. 2441-2453, Sep. 2005.
- [18] M. Lienard and P. Degauque, "Natural wave propagation in mine environments," *IEEE Trans. Antennas Propagat.*, vol. 48, pp. 1326-1339, Sep. 2000.

- [19] R. E. Collin, *Field Theory of Guided Waves*. New York: IEEE Press, 1991, ch. 5.



**Xiao Hong MAO** (S'09) received the B. Eng. (Hons) in Electrical and Electronics Engineering from the Nanyang Technological University, Singapore, in 2007, where she is working towards the Ph.D degree. She has been a Research Engineer in the School of Electrical and Electronic Engineering, Nanyang Technological University since September 2009. Her research interest is in channel modeling and characterization in complex environments.



**Yee Hui LEE** (S'96-M'02) received the B. Eng. (Hons) and M.Eng. degrees in Electrical and Electronics Engineering from the Nanyang Technological University, Singapore, in 1996 and 1998, respectively. She received her Ph.D. degree from the University of York, York, U.K., in 2002. Since July 2002, she has been an Assistant Professor at the School of Electrical and Electronic Engineering, Nanyang Technological University. Her interest is in channel characterization, rain propagation, antenna design, electromagnetic band gap structures, and evolutionary techniques.



**Boon Chong NG** (M'88-SM'06) received the B. Eng (Hons) in Electrical Engineering from the National University of Singapore in 1988. He had been with the Defence Science Organization (DSO), Singapore from 1988-1989 and 1990-1993 as a research engineer. He received the MSc in Electrical Engineering, MSc in Statistics, and PhD in Electrical Engineering, from Stanford University, USA in 1990, 1996 and 1998 respectively. He was the recipient of the Singapore Government DTTA postgraduate fellowship from 1993-1997 and was also a research assistant (1998) in the Information Systems Laboratory at Stanford University. Currently, he holds the appointment of Head of the Advanced Communications Laboratories and is a Principal Member of the Technical Staff at DSO National Laboratories, and is also an adjunct Associate Professor at the School of Electrical and Electronic Engineering, Nanyang Technological University. He leads research and development groups in MIMO communications, software and cognitive radios.